Synthesis and physical properties of $CeRu_2As_2$ and $CeIr_2As_2$

Kangqiao Cheng,[1] Xiaobo He,[1] Haiyang Yang,[2] Binjie Zhou,[1] Yuke Li,[2,*] and Yongkang Luo[1,†]

[1]*Wuhan National High Magnetic Field Center and School of Physics, Huazhong University of Science and Technology, Wuhan 430074, China*

[2]*Department of Physics and Hangzhou Key Laboratory of Quantum Matters, Hangzhou Normal University, Hangzhou 311121, China*

(Received 26 August 2019; revised manuscript received 8 October 2019; published 14 November 2019)

We studied the physical properties of two Kondo-lattice compounds, $CeRu_2As_2$ and $CeIr_2As_2$, by a combination of electric transport, magnetic, and thermodynamic measurements. They are of $ThCr_2Si_2$-type and $CaBe_2Ge_2$-type crystalline structures, respectively. $CeRu_2As_2$ shows localized long-range antiferromagnetic ordering below $T_N = 4.3$ K, with a moderate electronic Sommerfeld coefficient $\gamma_0 = 35$ mJ/mol K^2. A field-induced metamagnetic transition is observed near 2 T below T_N. Magnetic susceptibility measurements on aligned $CeRu_2As_2$ powders suggest that it has an easy axis and that the cerium moments align uniaxially along c axis. In contrast, $CeIr_2As_2$ is a magnetically nonordered heavy-fermion metal with enhanced $\gamma_0 > 300$ mJ/mol K^2. The initial onset Kondo temperatures of the two compounds are, respectively, 6 and 30 K. We discuss the role of the crystal structure to the strength of Kondo coupling. This paper provides two dense Kondo-lattice materials for further investigations on electronic correlation, quantum criticality, and heavy-electron effects.

DOI: 10.1103/PhysRevB.100.205121

I. INTRODUCTION

The hybridization (J_{cf}) between conduction (c) electrons and more localized f electrons in Kondo-lattice compounds simultaneously yields two competing phenomena: the Ruderman-Kittel-Kasuya-Yosida (RKKY) interaction [1–3] and the Kondo effect [4,5]. While the RKKY interaction mediates the magnetic exchange between local moments and stabilizes a long-range magnetic ordering, the consequence of Kondo effect is to screen and quench the local moments. Depending on the strength of J_{cf}, the ground state of Kondo lattices varies from the localized magnetic ordered regime for small J_{cf} to the heavy-fermion regime for moderate J_{cf} to the intermediate-valence regime for large J_{cf}.

"Ce-122" refers to a big family of Kondo-lattice compounds. It is mainly composed of two types of tetragonal crystalline structures: The $ThCr_2Si_2$ type ($I4/mmm$, no. 139) and $CaBe_2Ge_2$ type ($P4/nmm$, no. 129). We show their crystalline structures in Fig. 1(a). The discovery of superconductivity in K-doped $BaFe_2As_2$ rekindled the interest in the $ThCr_2Si_2$ structure [6]. In this structure, two vertically inverted CrSi layers are alternatingly sandwiched with Th ions embedded in between. Historically, $ThCr_2Si_2$ structure was also well known for hosting a number of Kondo-lattice materials (see reviews [7–9]), including $CeCu_2Si_2$, the first heavy-fermion superconductor [10]; URu_2Si_2, the hidden order superconductor [11]; $YbRh_2Si_2$, the Kondo breakdown quantum critical point [12]; etc. The $CaBe_2Ge_2$-type structure is relatively less famous. In this structure, the Be and Ge sites are interchanged in every other layer, and interlayer couplings can be bridged by Be-Ge bonding, which renders a more three-dimensional network than $ThCr_2Si_2$. Some examples are $CeRh_2P_2$ [13], $CeNi_2As_2$ [14], and $CeIr_2Si_2$ [15]. Note that $CeNi_2As_2$ can crystallize in both structures [14,16,17]. For $ThCr_2Si_2$- and $CaBe_2Ge_2$-type Ce-122, the Ce-4f electrons interact with the conduction electrons donated by CrSi and BeGe layers, respectively, and such a c-f hybridization builds up a natural platform to investigate Kondo effect and electronic correlations. A variety of interesting emergent states have been observed in Ce-122 compounds—e.g., metamagnetism, heavy fermions, non-Fermi liquids, quantum critical points (QCPs), and unconventional superconductivity [10,17–22]—the mechanisms of which remain controversial. In particular, local centrosymmetry is broken in $CaBe_2Ge_2$-type Ce-122, making it a candidate in the search for new noncentrosymmetric heavy-fermion superconductors. Extensive material bases are required in this field.

In this paper, we study two Ce-122 Kondo-lattice compounds, $CeRu_2As_2$ and $CeIr_2As_2$. The $ThCr_2Si_2$-type $CeRu_2As_2$ is a material developed for this paper. The synthesis of $CaBe_2Ge_2$-type $CeIr_2As_2$ has been reported by Pfannenschmidt *et al.* [23], but its physical properties have not been well studied. Our paper reveals that $CeRu_2As_2$ is a 4f-electron localized antiferromagnet with Néel temperature $T_N = 4.3$ K and a moderate Sommerfeld coefficient $\gamma_0 = 35$ mJ/mol K^2, whereas $CeIr_2As_2$ is a magnetically nonordered heavy-fermion metal with enhanced Sommerfeld coefficient $\gamma_0 > 300$ mJ/mol K^2. The initial onset Kondo temperatures of the two compounds are, respectively, 6 and 30 K. These results place them in the regimes of magnetically ordered with small J_{cf} and heavy fermion with moderate J_{cf}, respectively.

II. EXPERIMENTAL DETAILS

Polycrystalline $CeRu_2As_2$ and $CeIr_2As_2$ samples were synthesized by the method of solid-state reaction. High-purity Ce, Ru, Ir, and As were used as starting materials. First, CeAs,

*yklee@hznu.edu.cn
†mpzslyk@gmail.com

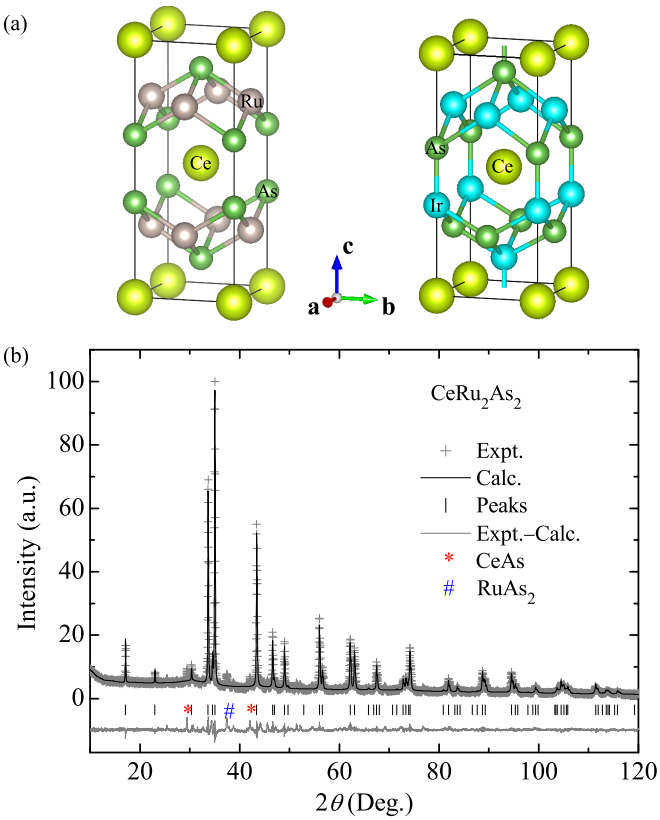

FIG. 1. (a) Crystalline structure of $ThCr_2Si_2$-type $CeRu_2As_2$ (left) and $CaBe_2Ge_2$-type $CeIr_2As_2$ (right). (b) Rietveld refinement of $CeRu_2As_2$ XRD pattern.

RuAs, and IrAs were prepared by reacting As powders with Ce, Ru, and Ir powders at 973, 1073, and 1273 K, respectively, for 24 h. Then, powders of CeAs, RuAs, and Ru were weighted according to the stoichiometric ratio, thoroughly ground, and pressed into a pellet under a pressure of 600 MPa in an argon-filled glove box. The pellet was packed into an alumina crucible and sealed into an evacuated quartz tube, which was then slowly heated to 1323 K and kept at that temperature for 48 h. After that, the resultant was reground and resintered two more times to achieve a good homogeneity. The synthesis for $CeIr_2As_2$ was essentially similar, while the sintering temperature was at 1373 K. The non-4f analogs $LaRu_2As_2$ and $LaIr_2As_2$ were also grown, by the same method.

Powder x-ray-diffraction (XRD) patterns were recorded at room temperature on a PANalytical x-ray diffractometer with Cu Kα radiation. Electrical resistivity was measured by standard four-probe method in a physical property measurement system (PPMS-9, Quantum Design), which was also used for the specific-heat measurements. Magnetization measurements were performed using a magnetic property measurement system (MPMS-VSM, Quantum Design). The measurements were made after a zero-field-cooling process.

III. RESULTS AND DISCUSSION

The crystalline structures of $CeRu_2As_2$ and $CeIr_2As_2$ are shown in Fig. 1. For the compound $CeRu_2As_2$, we performed the Rietveld refinement to the XRD. The peaks are well indexed to the tetragonal $ThCr_2Si_2$-type structure, except for a little impurity phase of CeAs and $RuAs_2$. The best fitting parameters are $a = 4.1696(5)$ Å, $c = 10.3868(7)$ Å, and the atomic coordinate of As [0, 0, 0.3692(4)]. More details about the structural parameters of $CeRu_2As_2$ and $CeIr_2As_2$ can be found in Table I. The lengths of a and c axes of $CeIr_2As_2$ obtained in this paper are close to but a little smaller than those in literature [23]. The Ir-As bonding ($d_{\text{Ir-As}} = 2.33$ Å) between adjacent IrAs layers makes the c axis much shorter than in $CeRu_2As_2$ ($d_{\text{As-As}} = 2.72$ Å).

TABLE I. Crystallographic parameters of $CeRu_2As_2$ from the Rietveld refinement to the powder x-ray diffractions at 300 K. The data of $CeIr_2As_2$ are also shown for comparison.

Parameter	Value	Value
Compound	$CeRu_2As_2$	$CeIr_2As_2$
Space group	$I4/mmm$	$P4/nmm$
a (Å)	4.1696(5)	4.2865(6)
c (Å)	10.3868(7)	9.8849(9)
V (Å^3)	180.580	181.625
Z	2	2
ρ (g/cm^3)	9.050	12.332
R_{wp} (%)	9.36	11.57

Figures 2(a) and 2(b) show the temperature dependence of magnetic susceptibility ($\chi = M/B$) of polycrystalline $CeRu_2As_2$ and $CeIr_2As_2$. For temperatures above 150 K, χ of both compounds obeys the standard Curie-Weiss formula, $\chi(T) = \frac{C}{T-\theta_W}$, where θ_W is the Weiss temperature. The fittings yield the effective moment $\mu_{\text{eff}} = 2.50$ and 2.56 μ_B for $CeRu_2As_2$ and $CeIr_2As_2$, respectively, very close to that of a free Ce^{3+} ion, 2.54 μ_B. This implies that the Ru and Ir ions are essentially nonmagnetic. The derived θ_W is -51 K for $CeRu_2As_2$, suggestive of antiferromagnetic correlation among Ce moments. A hump is seen near 80 K in $CeIr_2As_2$, which makes χ less temperature dependent at low temperature. Similar behavior was also seen in $CeCoIn_5$ and $CeIrIn_5$ [24], which is probably due to the crystalline electric field (CEF) effect (see below). For comparison, the magnetic susceptibility of $CeIr_2P_2$ (data reproduced from Ref. [23]) is also shown in Fig. 2. Pfannenschmidt *et al.* placed $CeIr_2P_2$ in the regime of intermediate valence, based on the Pauli-paramagnetic-like $\chi(T)$. Apparently, the "chemical pressure" effect of As-P substitution greatly enhances the c-f hybridization, and the 4f electrons become delocalized in $CeIr_2P_2$. At low temperature, the most prominent feature of $CeRu_2As_2$ is that $\chi(T)$ displays a sharp peak at 4.3 K, manifesting an antiferromagnetic (AFM) transition which will be studied further. No anomaly is seen in $CeIr_2As_2$ at low T; the slight increase in χ is probably due to some magnetic impurities (CeAs). We should point out that the fitted θ_W from the high-T region is ≈ -110 K for $CeIr_2As_2$, much larger than that of $CeRu_2As_2$. Since $CeIr_2As_2$ does not show any magnetic ordering, this enhanced θ_W is likely promoted by the Kondo effect. Further transport and specific-heat measurements suggest that $CeIr_2As_2$ sits much closer to a QCP.

In Fig. 2(c), we display $\chi(T)$ of $CeRu_2As_2$ under different magnetic fields. As field increases, the peak in $\chi(T)$ is

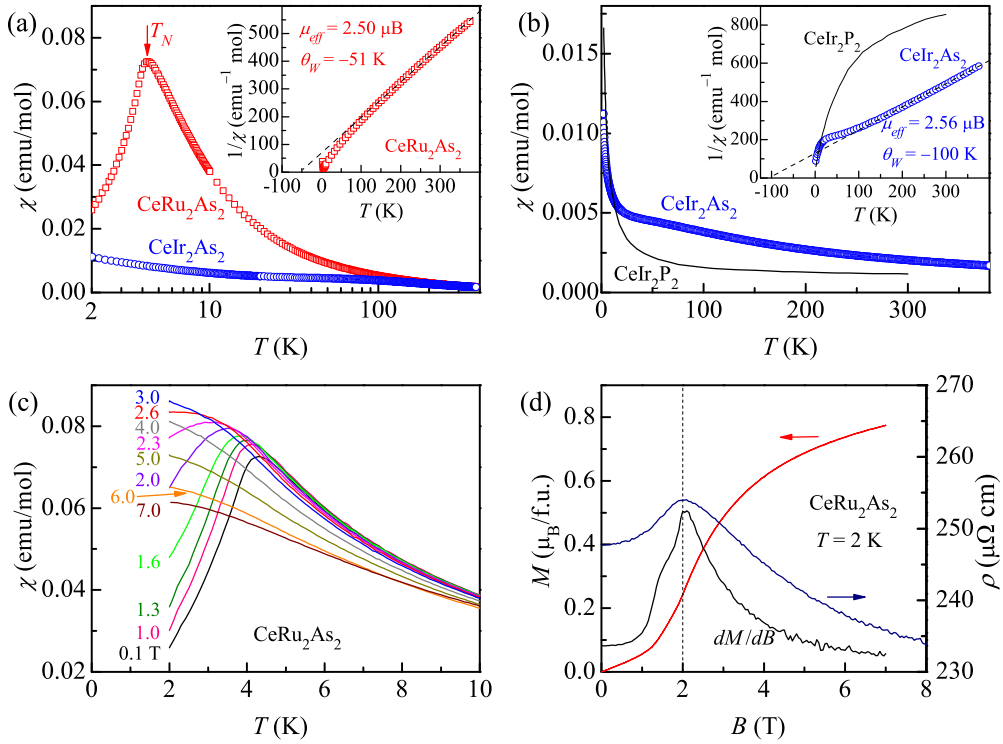

FIG. 2. (a), (b) Temperature-dependent magnetic susceptibility of polycrystalline $CeRu_2As_2$ and $CeIr_2As_2$. $CeRu_2As_2$ undergoes an AFM transition at $T_N = 4.3$ K. The insets display the Curie-Weiss fittings. The curve of $CeIr_2P_2$ (black line) reproduced from Ref. [23] is shown for comparison. (c) Evolution of the AFM peak in $\chi(T)$ of $CeRu_2As_2$ under various fields. (d) Field dependent magnetization (left), resistivity (right), and derivative susceptibility (dM/dB) of $CeRu_2As_2$ at 2 K.

gradually suppressed, and meanwhile the peak position also moves to lower temperature, characteristic of an AFM transition. For a field at about 2.6 T, the peak disappears, and $\chi(T)$ saturates at low temperature. Further increasing B, the value of magnetic susceptibility decreases systematically, and no clear anomaly is seen in $\chi(T)$ except for a trend of saturation at low T. Such an evolution with field typically entails a field-induced metamagnetic transition, as observed in many cerium compounds [17,25]. Since Ce^{3+} has a small de Gennes factor [26], the magnetic exchange coupling between cerium moments is generally weak; thus, the magnetic moments can be reoriented by a moderate field. This is indeed the case in $CeRu_2As_2$. In Fig. 2(d), we present isothermal field dependent magnetization and derivative susceptibility (dM/dB) at 2 K. Under low field, the magnetization increases linearly. A speedup is visible for fields larger than 1 T, and finally tends to saturate above 4 T. This trend is more clearly seen in dM/dB that peaks near 2 T. Similar metamagnetic transition was interpreted as a spin flop in $CeNi_2As_2$ where the magnetic moments are uniaxially aligned along c and a tiny hysteresis is seen near the metamagnetic transition [17]. In $CeRu_2As_2$, the hysteresis is negligible, probably due to the polycrystalline sample.

To further study the magnetic anisotropy of $CeRu_2As_2$, we measured the susceptibility of field-aligned powders. The polycrystalline sample was thoroughly ground into powders (this process was carried out carefully in a glove box), and mixed with Stycast 1266 epoxy with a small weight ratio ≈0.2 so that the grains are well isolated by epoxy [27]. The mixture was then placed in a strong aligning field ($\mathbf{B_{al}}$) of 14 T at 300 K in a PPMS and held motionless for 12 h before the Stycast was completely cured. The magnetic susceptibility for fields parallel ($\chi_\parallel$) and perpendicular ($\chi_\perp$) to $\mathbf{B_{al}}$ is shown in Fig. 3 as a function of T. (Refer to the Appendix for more details.) The important findings are as follows.

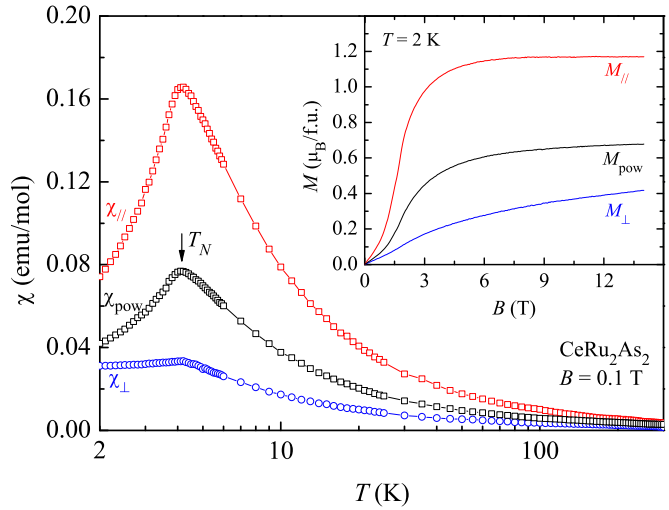

FIG. 3. Temperature dependence of $\chi_\parallel$ and $\chi_\perp$ measured from aligned $CeRu_2As_2$ powders. The inset shows the isothermal field dependent magnetization. $\parallel$ and $\perp$ correspond to the aligning field $\mathbf{B_{al}}$. See the Appendix. The results for unaligned powders (χ_{pow}) are shown for comparison.

(i) $\chi_\perp$ is much smaller than $\chi_\parallel$, indicative of strong magnetic anisotropy. In particular, we notice the value of $\chi_\perp$ is less than half of $\chi_\parallel$ over the full range 2–300 K; for instance, at 300 K, $\chi_\parallel = 3.65 \times 10^{-3}$ emu/mol and $\chi_\perp = 1.66 \times 10^{-3}$ emu/mol. This suggests that the compound has an easy axis, rather than an easy plane, because for the latter case $\chi_\parallel = \chi_{a,b}$ and $\chi_\perp = (\chi_{a,b} + \chi_c)/2$ (see the Appendix); $\chi_\perp < \chi_\parallel/2$ is not likely for cerium-contained compounds.

(ii) At low temperature, a sharp peak is seen at T_N in $\chi_\parallel$, characteristic of an AFM transition. In contrast, the peak in $\chi_\perp$ is very shallow, and the susceptibility tends to saturate below T_N. These features are highly suggestive that in the AFM state the Ce moments are uniaxially along the easy axis.

(iii) The inset to Fig. 3 shows field dependent magnetization of aligned powders at 2 K. $M_\parallel$ increases with field rapidly and saturates at 1.17 μ_B under high magnetic field. The metamagnetic transition is obviously seen in $M_\parallel$, even sharper than in unaligned powders ($M_{\rm pow}$). $M_\perp$ is much smaller than $M_\parallel$ and keeps increasing at 14 T. A little sign of metamagnetic transition is also visible in $M_\perp$, which probably arises from a small portion of unaligned powders.

In light of these observations, it is reasonable to propose c as the easy axis of $CeRu_2As_2$, and below T_N the magnetic moments also align antiferromagnetically along c. This makes a field-induced spin flop possible. In fact, the dM/dB in Fig. 2(d) shows a small shoulder before 2 T, which potentially points to a secondary transition prior to the polarized paramagnetic state. Given an easy-axis antiferromagnet, this secondary transition might be a signature for an intermediate spin-flop phase. Of course, to get a precise magnetic structure, high-quality single crystals and microscopic measurements like neutron-scattering experiments are needed. CEF effect often plays a key role in such a magnetic anisotropy in cerium compounds.

The resistivities (ρ) of $CeRu_2As_2$ and $CeIr_2As_2$ and their La counterparts are presented in Fig. 4. A previous work on $LaRu_2As_2$ by Guo *et al.* has revealed metallic behavior and a superconducting transition at $T_c = 7.8$ K [28], and these features are well reproduced in the current paper. For

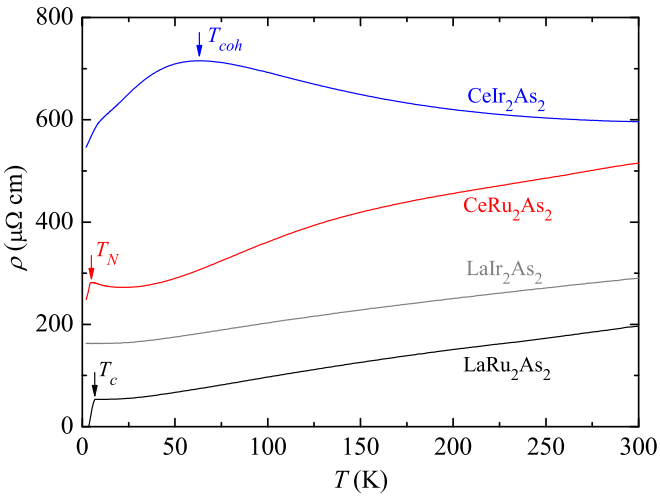

FIG. 4. Temperature dependent electric resistivity of $CeRu_2As_2$, $CeIr_2As_2$, $LaRu_2As_2$, and $LaIr_2As_2$.

$CeRu_2As_2$, $\rho(T)$ shows a hump around 150 K, which should be a consequence of CEF splitting of the Ce^{3+} $j = 5/2$ multiplet. $\rho(T)$ slightly turns up below 22 K, and then decreases sharply below 4.3 K, reminiscent of reduction in spin scattering due to the formation of long-range AFM ordering. $LaIr_2As_2$ behaves like a simple metal; i.e., upon cooling down, $\rho(T)$ decreases almost linearly above 100 K, and then tends to flatten by showing some T^2-like behavior at low temperature, characteristic of Fermi liquid. The large residual resistivity ρ_0 is probably because of the sample quality. In contrast, $CeIr_2As_2$ exhibits the typical dense Kondo behavior (see, e.g., $CeIrIn_5$ [29,30]): $\rho(T)$ initially increases as T decreases, and then turns down rapidly after passing through a broad peak near $T_{\rm coh} = 63$ K. $T_{\rm coh}$ designates a crossover from the incoherent Kondo scattering regime for $T > T_{\rm coh}$ where Ce moments behave like separate single-ion impurities to the coherent Kondo scattering regime for $T < T_{\rm coh}$ where the Ce-4f electrons develop strongly correlated bands. At low temperature, $\rho(T)$ keeps decreasing linearly down to 2 K, the base temperature of our measurements, without restoring any signature of Fermi-liquid behavior. This places $CeIr_2As_2$ in a regime of non-Fermi liquid or "strange metal" [7] which is usually observed in the vicinity of a quantum critical point [12,31–34]. Sub-Kelvin measurements are needed in the future to further clarify this issue.

For $CeRu_2As_2$, we also took a field dependent resistivity measurement at 2 K (below T_N), as shown in Fig. 2(d). Under low field, ρ increases with field, because external magnetic field disturbs the long-range AFM ordering and causes more spin scattering. A maximum is seen in $\rho(B)$ at 2 T, and after that the resistivity decreases again. The critical field 2 T is coincident with the field at which $M(B)$ shows the largest slope and dM/dB peaks. Further increasing B, spin scattering is reduced as the moments are gradually polarized, and thus the resistivity decreases.

Turning now to the specific heat, for both $CeRu_2As_2$ and $CeIr_2As_2$ we subtract, respectively, the specific heat of $LaRu_2As_2$ (measured under a field of 1 T) and $LaIr_2As_2$, and the resultants are the contribution from 4f electrons, C_{4f}. Figure 5(a) shows C_{4f}/T of $CeRu_2As_2$ as a function of T. A λ-shape peak is clearly seen at the transition temperature T_N, manifesting a second-order phase transition. A small substructure is seen between 6 and 9 K, which should be from some CeAs impurity that undergoes an AFM transition at 7.6 K [35]. The Sommerfeld coefficient γ_0 estimated from the paramagnetic state is 35 mJ/mol K^2, in line with the well-localized and ordered 4f electrons. We calculated the magnetic entropy ($S_{\rm mag}$) by integrating C_{4f}/T over T. For the low-temperature part, we have linearly extrapolated the C_{4f}/T to $T \to 0$ limit to ensure $S_{\rm mag}(0) = 0$, and the result is plotted in the inset to Fig. 5(a). The entropy gain is about 73% $R \ln 2$ at T_N, and fully recovers $R \ln 2$ at 12 K. The initial onset Kondo temperature can be estimated as $T_0 \simeq 6$ K through a widely accepted criterion $S_{\rm mag}(T_0/2) = 0.4\, R \ln 2$ [36]. For $CeIr_2As_2$, C_{4f}/T turns up logarithmically at low temperature, and tends to level off below 1 K. This suggests that the Fermi-liquid behavior likely restores at low temperature with greatly enhanced quasiparticle effective mass and Sommerfeld coefficient $\gamma_0 > 300$ mJ/mol K^2. Such behavior is usually seen in systems beyond but close to a QCP [37–39]. The estimated T_0

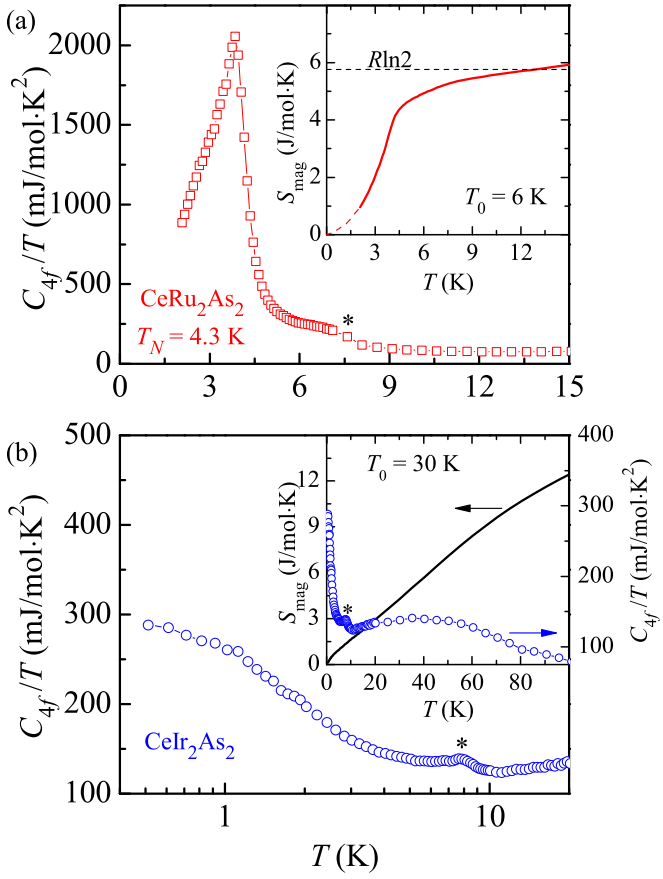

FIG. 5. The $4f$-electron contribution to specific heat divided by temperature, C_{4f}/T, as a function of T of $CeRu_2As_2$ (a) and $CeIr_2As_2$ (b). The insets show the magnetic entropy derived by integrating C_{4f}/T over T. A broad maximum seen in C_{4f}/T of $CeIr_2As_2$ near 40 K indicates ≈90 K of the first CEF splitting, which is consistent with what is seen in $\chi(T)$. The "*" in both panels designate the anomalies due to CeAs impurity.

is about 30 K, much larger than that of $CeRu_2As_2$, demonstrating stronger Kondo coupling. We should also mention that C_{4f}/T displays a broad maximum near 40 K [see the right frame of the inset to Fig. 5(b)]. Such a broad peak arises from the Schottky anomaly, which is a consequence of CEF splitting. The six-degenerated $j = 5/2$ multiplet splits into three doublets in the presence of tetragonal CEF. The energy difference between the first excited and ground doublets is expected to be ≈90 K in this case, which agrees well with the hump observed in magnetic susceptibility [see Fig. 2(b)].

These physical properties above enable us to place $CeRu_2As_2$ and $CeIr_2As_2$, respectively, in the regime of magnetically ordered for small J_{cf} and heavy fermion for moderate J_{cf}. Aside from those, $CeIr_2P_2$ sits in the intermediate-valence regime with strong J_{cf}. First, it is worthwhile to make a rough estimate of cerium valence through the bond-valence theory. The original idea was proposed by Brown [40] and Brown and Altermatt [41], and the valence of an ion in the compound is a function of the bond lengths d_{ij}:

$$V_i = \sum_j v_{ij}, \tag{1}$$

where v_{ij} can be expressed in terms of d_{ij} [42]:

$$v_{ij} = \exp[(R_{ij} - d_{ij})/b]. \tag{2}$$

Here b is commonly taken to be a "universal" constant close to 0.37 Å, while R_{ij} is called the bond-valence parameter and is taken as 2.78 Å for Ce-As bonding and 2.70 Å for Ce-P bonding [42]. According to the crystalline parameters, we get the cerium valences +2.27, +2.28, and +2.53 for $CeRu_2As_2$, $CeIr_2As_2$, and $CeIr_2P_2$, respectively. These values apparently are underestimated as compared to $Ce^{3+/4+}$, because we only take into account the Ce-As(P) bonding with nearest neighbor. However, what is important here is the following.

(i) The cerium valence in $CeIr_2P_2$ is much higher than in $CeIr_2As_2$, in line with the fact that $CeIr_2P_2$ has an intermediate valence.

(ii) The calculated cerium valences are essentially the same in $CeRu_2As_2$ and $CeIr_2As_2$.

This indicates that the transition metal is crucial to the physical properties of $CeTm_2As_2$. Indeed, $5d$ orbitals are more extended in space than $4d$ orbitals, and this makes the c-f hybridization more effective in $CeIr_2As_2$. Apart from this, as we already mentioned, the $CaBe_2Ge_2$-type $CeIr_2As_2$ has the interlayer Ir-As bonding, and this results in a three-dimensional Ir-As network, and, correspondingly, Kondo coupling is more efficient. A more straightforward case is $CeNi_2As_2$, which has both types of crystal structures [14]. While the $ThCr_2Si_2$-type $CeNi_2As_2$ is an antiferromagnet with $T_N \approx 5$ K [17], the $CaBe_2Ge_2$-type $CeNi_2As_2$ is nonmagnetic due to Kondo effect [16]. We argue that for these two reasons the $CaBe_2Ge_2$-type $CeIr_2As_2$ exhibits much stronger Kondo effect and electronic correlation than the $ThCr_2Si_2$-type $CeRu_2As_2$.

IV. CONCLUSIONS

To summarize, we investigated the physical properties of two Ce-122 Kondo lattice compounds, $ThCr_2Si_2$-type $CeRu_2As_2$ and $CaBe_2Ge_2$-type $CeIr_2As_2$. We find that $CeRu_2As_2$ is a local-moment antiferromagnet with Néel temperature $T_N = 4.3$ K, Sommerfeld coefficient $\gamma_0 = 35$ mJ/mol K^2, and initial onset Kondo temperature $T_0 \approx 6$ K. The cerium moments are assumed to be uniaxially aligned along c, which is also proposed as the easy axis. $CeIr_2As_2$ appears to reside on the nonmagnetic side of a quantum critical point, exhibiting heavy-electron effect with enlarged $\gamma_0 >$ 300 mJ/mol K^2 and $T_0 \approx 30$ K. This paper, therefore, provides two dense Kondo-lattice materials for further studying electronic correlation, quantum criticality, and heavy-electron effects. High-quality single crystals are highly needed in the future.

ACKNOWLEDGMENTS

The authors acknowledge J. D. Thompson and J. Bao for helpful discussions. Y. Luo acknowledges 1000 Youth Talents Plan of China. Y. Li is supported by National Natural Science Foundation of China (Grant No. U1932155).

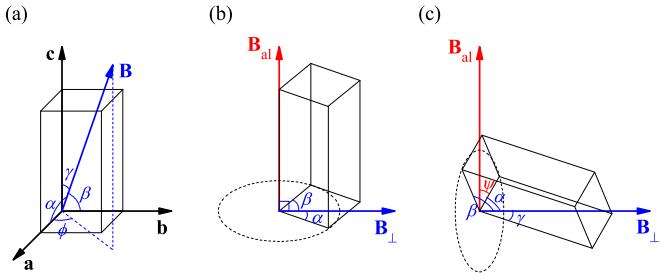

FIG. 6. (a) External magnetic field **B** applied in an arbitrary direction with respect to the *tetragonal* unit cell. α, β, and γ are the angles between **B** and the principal axes, and ϕ is the angle spanned by a and the projection of **B** in the ab plane. (b) For the easy-axis case, c is along the aligning field $\mathbf{B}_{al}$. (c) For the easy-plane case, $\mathbf{B}_{al}$ is inside the ab plane, and c is perpendicular to $\mathbf{B}_{al}$. $\mathbf{B}_{\perp}$ ($\mathbf{B}_{\parallel}$, not shown) is the field applied perpendicular (parallel) to $\mathbf{B}_{al}$ to measure $m_{\perp}$ ($m_{\parallel}$).

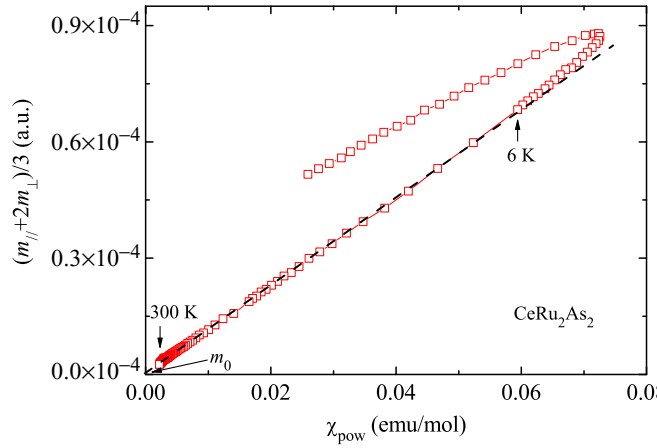

FIG. 7. $(m_{\parallel}+2m_{\perp})/3$ vs χ_{pow} with T as an implicit parameter. The slope is determined by the weight of aligned $CeRu_2As_2$ powders.

APPENDIX: MAGNETIC SUSCEPTIBILITY FOR ALIGNED POWDERS

To start with, we deduce the formulas of magnetic susceptibility of polycrystalline powders. Assuming an arbitrary magnetic field **B** is applied to a tetragonal unit cell (e.g., $CeRu_2As_2$), the direction of field is characterized by α, β, and γ as shown in Fig. 6(a). The magnetic susceptibility in such configuration is $\chi(\alpha,\beta,\gamma)=\chi_a\cos^2\alpha+\chi_b\cos^2\beta+\chi_c\cos^2\gamma$ [43]. Note that $\chi_a=\chi_b$ for tetragonal symmetry. Taking the powder average, we derive the susceptibility for a bulk polycrystal:

$$\chi_{pow}=\frac{\iint\chi(\alpha,\beta,\gamma)\sin\gamma d\gamma d\phi}{\int_0^{2\pi}\int_0^{\pi}\sin\gamma d\gamma d\phi}=\frac{\chi_a+\chi_b+\chi_c}{3}, \quad \text{(A1)}$$

where ϕ is the angle between a and the projection of **B** in the ab plane.

Now considering that the powder is aligned by an aligning field $\mathbf{B}_{al}$, we have the following.

(1) For an easy-axis case [Fig. 6(b)], c will be aligned to $\mathbf{B}_{al}$, and one easily finds $\chi_{\parallel}=\chi_c$, while $\chi_{\perp}=\chi_{a,b}$. Here, the notations $\parallel$ and $\perp$ correspond to $\mathbf{B}_{al}$.

(2) For an easy-plane case [Fig. 6(c)], the ab plane will be parallel with $\mathbf{B}_{al}$, while c lays inside the plane perpendicular to $\mathbf{B}_{al}$. The angle between a and $\mathbf{B}_{al}$ is named ψ. In this case, $\chi_{\parallel}=\chi_{a,b}$, while $\chi_{\perp}$ is

$$\chi_{\perp}=\frac{\iint\chi(\alpha,\beta,\gamma)\sin\psi d\psi d\gamma}{\int_0^{2\pi}\int_0^{\pi}\sin\psi d\psi d\gamma}=\frac{\chi_{a,b}+\chi_c}{2}. \quad \text{(A2)}$$

Equation (A2) can be deduced, because $\cos\alpha=\sin\psi\sin\gamma$, and $\cos\beta=-\cos\psi\sin\gamma$. Interestingly, for both easy-axis and easy-plane cases,

$$\chi_{\parallel}+2\chi_{\perp}=\chi_a+\chi_b+\chi_c=3\chi_{pow}. \quad \text{(A3)}$$

Equation (A3) enables us to figure out the weight of aligned powers in the mixture. In Fig. 7 we plot $(m_{\parallel}+2m_{\perp})/3$ vs χ_{pow} where T is the implicit parameter. The plot shows good linearity for T above 6 K. The intercept of this linear scaling, m_0, should be attributed to Stycast (which we assume is isotropic and temperature independent), and the slope is determined by the weight of the aligned powders. After subtracting m_0 from $m_{\parallel}$ and $m_{\perp}$, and with the slope, we are able to convert magnetization into magnetic susceptibility, as shown in Fig. 3(a).

[1] M. A. Ruderman and C. Kittel, Phys. Rev. **96**, 99 (1954).
[2] T. Kasuya, Prog. Theor. Phys. **16**, 45 (1956).
[3] K. Yosida, Phys. Rev. **106**, 893 (1957).
[4] J. Kondo, Prog. Theor. Phys **32**, 37 (1964).
[5] A. C. Hewson, *The Kondo Problem to Heavy Fermions* (Cambridge University, Cambridge, England, 1993).
[6] M. Rotter, M. Tegel, and D. Johrendt, Phys. Rev. Lett. **101**, 107006 (2008).
[7] G. R. Stewart, Rev. Mod. Phys. **73**, 797 (2001).
[8] P. Misra, *Handbook of Metal Physics: Heavy-Fermion Systems* (Elsevier, Amsterdam, 2008).
[9] C. Pfleiderer, Rev. Mod. Phys. **81**, 1551 (2009).
[10] F. Steglich, J. Aarts, C. D. Bredl, W. Lieke, D. Meschede, W. Franz, and H. Schäfer, Phys. Rev. Lett. **43**, 1892 (1979).
[11] T. T. M. Palstra, A. A. Menovsky, J. van den Berg, A. J. Dirkmaat, P. H. Kes, G. J. Nieuwenhuys, and J. A. Mydosh, Phys. Rev. Lett. **55**, 2727 (1985).
[12] J. Custers, P. Gegenwart, H. Wilhelm, K. Neumaier, Y. Tokiwa, O. Trovarelli, C. Geibel, F. Steglich, C. Pepin, and P. Coleman, Nature (London) **424**, 524 (2003).
[13] R. Madar, P. Chaudouet, J. Senateur, S. Zemni, and D. Tranqui, J. Less Common Met. **133**, 303 (1987).
[14] E. E. Ghadraoui, J. Pivan, R. Guérin, O. Pena, J. Padiou, and M. Sergent, Mater. Res. Bull. **23**, 1345 (1988).
[15] K. Hiebl, C. Horvath, and P. Rogl, J. Less Common Met. **117**, 375 (1986).
[16] H. Suzuki, H. Abe, H. Kitazawa, and D. Schmitt, J. Alloys Compd. **323-324**, 520 (2001).

[17] Y. Luo, J. Bao, C. Shen, J. Han, X. Yang, C. Lv, Y. Li, W. Jiao, B. Si, C. Feng, J. Dai, G. Cao, and Z.-a. Xu, Phys. Rev. B **86**, 245130 (2012).
[18] J. Flouquet, P. Haen, S. Raymond, D. Aoki, and G. Knebel, Physica B **319**, 251 (2002).
[19] H. Q. Yuan, F. M. Grosche, M. Deppe, C. Geibel, G. Sparn, and F. Steglich, Science **302**, 2104 (2003).
[20] F. Grosche, S. Julian, N. Mathur, and G. Lonzarich, Physica B **223-224**, 50 (1996).
[21] R. Movshovich, T. Graf, D. Mandrus, J. D. Thompson, J. L. Smith, and Z. Fisk, Phys. Rev. B **53**, 8241 (1996).
[22] Y. Luo, F. Ronning, N. Wakeham, X. Lu, T. Park, Z. A. Xu, and J. D. Thompson, Proc. Natl. Acad. Sci. USA **112**, 13520 (2015).
[23] U. Pfannenschmidt, F. Behrends, H. Lincke, M. Eul, K. Schäfer, H. Eckert, and R. Pöttgen, Dalton Trans. **41**, 14188 (2012).
[24] C. Petrovic, P. G. Pagliuso, M. F. Hundley, R. Movshovich, J. L. Sarrao, J. D. Thompson, Z. Fisk, and P. Monthoux, J. Phys.: Condens. Matter **13**, L337 (2001).
[25] E. D. Mun, S. L. Bud'ko, A. Kreyssig, and P. C. Canfield, Phys. Rev. B **82**, 054424 (2010).
[26] S. Blundell, *Magnetism in Condensed Matter* (Oxford University, New York, 2001).
[27] B.-L. Young, M. S. Rose, D. E. MacLaughlin, K. Ishida, O. O. Bernal, H. G. Lukefahr, K. Heuser, E. J. Freeman, and M. B. Maple, Rev. Sci. Instrum. **73**, 3038 (2002).
[28] Q. Guo, B.-J. Pan, J. Yu, B.-B. Ruan, D.-Y. Chen, X.-C. Wang, Q.-G. Mu, G.-F. Chen, and Z.-A. Ren, Sci. Bull. **61**, 921 (2016).
[29] C. Petrovic, R. Movshovich, M. Jaime, P. G. Pagliuso, M. F. Hundley, J. L. Sarrao, Z. Fisk, and J. D. Thompson, EPL **53**, 354 (2001).
[30] Y. Takaesu, N. Aso, Y. Tamaki, M. Hedo, T. Nakama, K. Uchima, Y. Ishikawa, K. Deguchi, and N. K. Sato, J. Phys.: Conf. Ser. **273**, 012058 (2011).
[31] H. v. Löhneysen, C. Pfleiderer, T. Pietrus, O. Stockert, and B. Will, Phys. Rev. B **63**, 134411 (2001).
[32] T. Park, V. A. Sidorov, F. Ronning, J. X. Zhu, Y. Tokiwa, H. Lee, E. D. Bauer, R. Movshovich, J. L. Sarrao, and J. D. Thompson, Nature (London) **456**, 366 (2008).
[33] J. Custers, K.-A. Lorenzer, M. Müller, A. Prokofiev, A. Sidorenko, H. Winkler, A. M. Strydom, Y. Shimura, T. Sakakibara, R. Yu, Q. Si, and S. Paschen, Nat. Mater. **11**, 189 (2012).
[34] Y. Luo, L. Pourovskii, S. E. Rowley, Y. Li, C. Feng, A. Georges, J. Dai, G. Cao, Z. Xu, Q. Si, and N. P. Ong, Nat. Mater. **13**, 777 (2014).
[35] T. Suzuki, Y. S. Kwon, S. Ozeki, Y. Haga, and T. Kasuya, J. Mag. Mag. Mater. **90-91**, 493 (1990).
[36] P. Gegenwart, Q. Si, and F. Steglich, Nat. Phys. **4**, 186 (2008).
[37] E. M. Brüning, C. Krellner, M. Baenitz, A. Jesche, F. Steglich, and C. Geibel, Phys. Rev. Lett. **101**, 117206 (2008).
[38] Y. Luo, Y. Li, S. Jiang, J. Dai, G. Cao, and Z.-a. Xu, Phys. Rev. B **81**, 134422 (2010).
[39] L. Wang, Z. Fu, J. Sun, M. Liu, W. Yi, C. Yi, Y. Luo, Y. Dai, G. Liu, Y. Matsushita, K. Yamaura, L. Lu, J.-G. Cheng, Y. feng Yang, Y. Shi, and J. Luo, npj Quantum Mater. **2**, 36 (2017).
[40] I. D. Brown, *Structure and Bonding in Crystals* (Academic, New York, 1981), Vol. 2.
[41] I. D. Brown and D. Altermatt, Acta Cryst. B **41**, 244 (1985).
[42] N. E. Brese and M. O'Keeffe, Acta Cryst. B **47**, 192 (1991).
[43] P. Boutron, Phys. Rev. B **7**, 3226 (1973).